DR MICHAEL P SCHMITT (Orcid ID : 0000-0003-0922-3975)

Article type : Article

Corresponding author mail id :- m.schmitt@hamrindustries.com

Durable Aluminate Toughened Zirconate Composite Thermal Barrier Coating (TBC) Materials for High Temperature Operation

Michael P. Schmitt[1], Jamesa L. Stokes[2,3], Amarendra K. Rai[4], Andrew J. Schwartz[2,3], Douglas E. Wolfe[2,3,5]

[1] HAMR Industries LLC, 1315 W. College Ave, Suite 301, State College, PA 16801, USA

[2] Department of Materials Science and Engineering, 221 Steidle Building, The Pennsylvania State University, University Park, PA 16802, USA

[3] The Applied Research Laboratory, 230 Innovation Blvd., The Pennsylvania State University, University Park, PA 16802, USA

[4] UES Inc. 4401 Dayton Xenia Road, Dayton, OH 45432, USA

[5] Department of Engineering Science and Mechanics, 212 Earth and Engineering Sciences Building, The Pennsylvania State University, University Park, PA 16802, USA

Abstract

Research on advanced thermal barrier coating (TBC) materials capable of operating beyond 1200°C has primarily focused on the rare earth zirconate pyrochlores, particularly gadolinium zirconate ($Gd_2Zr_2O_7$ – GZO). The drawback of this material is a significant reduction in durability due to a low fracture toughness. This study investigates utilization of a thermodynamically compatible gadolinia alumina perovskite ($GdAlO_3$ – GAP) toughening phase to improve the durability of GZO. Dense pellets were fabricated to assess the material properties with minimal microstructural influence. Thermal stability, elastic modulus, hardness, indentation fracture resistance and erosion durability were evaluated for GZO, GAP, and composite pellets containing 10, 30, and 50 wt.% GAP. It was demonstrated that GAP and GZO are thermodynamically compatible through 1600°C and thus capable of operating well beyond the limits of traditional 7 wt.% yttria stabilized zirconia (YSZ). Grain sizes are maintained due to a lack of diffusion, and thus microstructural stability is enhanced. The GAP fracture toughness was shown to be over 2X that of GZO while exhibiting a lower elastic modulus and similar hardness. The 50:50 GZO-GAP composite exhibited a 63% reduction in the absolute erosion rate, demonstrating the immense toughening capabilities of this system. The implications for composite TBCs utilizing this system are discussed, along with future work.

Keywords

Thermal Barrier Coatings (TBC), Aluminates, Durability, Composites, gadolinium zirconate (GZO)

1. Introduction

The next generation of thermal barrier coatings (TBCs) are sought to replace 7 wt.% yttria stabilized zirconia (7YSZ). The most commonly studied advanced TBC compositions are based on the rare earth zirconate pyrochlore family ($RE_2Zr_2O_7$). In particular, gadolinium zirconate ($Gd_2Zr_2O_7$ - GZO) is a leading candidate due to its phase stability up to 1550°C and ~2600°C for the pyrochlore and fluorite polymorphs, respectively (1). GZO also has a

significantly lower bulk thermal conductivity (1.4 W/m·K) than 7YSZ (2.2 W/m·K) (2), good thermal cyclic durability (when utilizing the appropriate 7YSZ interlayer to prevent interaction with the Al_2O_3 TGO), and improved resistance to calcium-magnesium-alumino-silicate (CMAS) degradation (3), a necessary criterion for materials operating above the ~1200°C capability threshold of 7YSZ. The primary drawback of GZO is that it possesses a low fracture toughness of ~1 MPa√m (4) which reduces erosion durability by an order of magnitude compared to that of 7YSZ (5). Therefore, a means of improving the erosion durability of pyrochlore materials must be developed if they are to be adapted for TBC applications in particulate laden environments.

Two methods present themselves for enhancing the durability of GZO-based coatings: (i) modifying the intrinsic toughness of GZO and/or (ii) modifying the extrinsic toughness of the coating system by changing the morphology or design architecture. A direct comparison of these approaches has been carried out by the authors and demonstrated the strengths and weaknesses of each method (6). For the intrinsic approach, several authors have investigated the effects of RE zirconate chemistry and stoichiometry on toughness (4,7–9). Unfortunately, the changes are not well understood and still result in toughness values significantly lower than that of 7YSZ, ultimately limiting their applicability. Conversely, extrinsically modifying the apparent toughness by incorporating secondary toughening phases has been previously shown by the authors to produce significant improvements in the erosion durability for two design architectures (multilayer and composite) (5,6,10–12). It was shown that by incorporating a secondary phase with higher toughness, the overall durability of the coating system was improved. Furthermore, the erosion durability improvements in the composite coatings exhibited a non-volumetric effect in which small additions had a large impact on coating performance. Previous work utilized a RE-modified YSZ (t' Low-k) as the toughening phase, which exhibits erosion durability roughly equivalent to that of 7YSZ (5), but with lower thermal conductivity and slightly higher phase stability. Unfortunately, this material is neither phase stable to 1400°C for prolonged periods of time, nor thermochemically compatible with GZO (5). For the composite approach to show long term viability, the secondary toughening phase should exhibit a high fracture toughness, high temperature phase stability to the desired temperature region, and thermochemical compatibility with the primary matrix phase (GZO in this case).

The present study investigates utilizing composites of GZO and gadolinia alumina perovskite ($GdAlO_3$ - GAP) in varying weight fractions to impart improved erosion durability

with respect to monolithic GZO. GAP is a member of the RE aluminate family, a group of materials which can exhibit high melting temperatures of up to 2500°C, and improved toughness with respect to the RE zirconates (13). Most importantly, the RE aluminates have thermochemical stability with the pyrochlore zirconates (1,14,15), as shown in the Gd_2O_3-ZrO_2-Al_2O_3 system (Figure 1). In addition to thermodynamic compatibility with GZO, GAP possesses phase stability up to its melting temperature of ~2045°C, as well as a reportedly high fracture toughness (13). This high fracture toughness has been attributed to plasticity near the crack tip, and therefore a form of ductility in the material (16). Thus, a GZO-GAP composite represents a materials system that has high temperature phase stability, thermochemical compatibility, and the potential to mitigate the low erosion durability of the RE zirconates, and in particular, GZO. This study explores the thermal and mechanical properties of the GZO-GAP composite system as a possible high temperature, phase stable replacement for current TBC systems. Composite pellets were fabricated with 10 wt.%, 30 wt.%, and 50 wt.% GAP additions to a GZO matrix, with monolithic GAP and GZO pellets serving as baselines. Dense pellets were utilized to isolate the impact of morphology on performance and enable a baseline for future comparison with porous coatings. A minimum of 50 wt.% GZO was explored in this study to maintain the beneficial properties of GZO (e.g. high temperature phase stability, low thermal conductivity, and CMAS resistance) while improving erosion performance.

2. Experimental Procedure

Spray-dried thermal spray powders of GZO (SkyWorks, Inc.) and GAP (SkyWorks, Inc.) were used as starting powders. The powders were first milled separately using 7 mm cylindrical YSZ media in ethanol, followed by subsequent milling with 2 mm spherical YSZ media in ethanol to achieve particle sizes of ~500 nm. To fabricate the composite pellets, the GZO and GAP powders were mixed in their respective weight ratios in ethanol with 2 mm spherical YSZ media to promote homogenization and prevent agglomeration prior to pressing. Three composite pellet compositions were fabricated in this study: 90 wt.% GZO:10 wt.% GAP, 70 wt.% GZO:30 wt.% GAP, and 50 wt.% GZO:50 wt.% GAP. These composite compositions are referred to as 90:10, 70:30 and 50:50 throughout this study. The powders were uniaxially pressed at 19.7 MPa into 25.4 mm diameter by 4 mm thick pellets before cold isostatic pressing (CIP) at 200 MPa with no hold at pressure. The pellets were then sintered at 1600°C for 24 hours to obtain dense

samples. Monolithic GZO and GAP pellets were fabricated similarly as baseline samples. Two batches of samples were fabricated under these conditions, with one set utilized for testing the thermal stability and the other utilized for evaluation of mechanical properties. The densities of the sintered samples were determined using the Archimedes method.

Elastic (E), shear (G), and bulk (K) moduli were obtained by an ultrasonic pulse/echo method. Longitudinal (V_L) and shear (V_S) wave velocities were measured through the pellet thickness to calculate the elastic properties using Equations 1 through 4:

$$G = \rho V_S^2 \tag{1}$$

$$E = \frac{G(3V_L^2 - 4V_S^2)}{V_L^2 - V_S^2} \tag{2}$$

$$K = \frac{E}{3-6\nu} \tag{3}$$

$$\nu = \frac{1-2\frac{V_S}{V_L}^2}{2-2\frac{V_S}{V_L}^2} \tag{4}$$

where ρ is the sample density and υ is Poisson's ratio, which is calculated using Equation 4.

Hardness (H) and indentation fracture resistance (K_{IFR}) measurements were obtained using a Vickers microhardness indenter (LECO M-400-G1 Hardness Tester, ASTM E384) at 1 kg load. The hardness and indentation fracture resistance, respectively, were calculated using:

$$H = \frac{1.854F}{d^2} \tag{5}$$

$$K_{IFR} = \frac{0.018F\sqrt{\frac{E}{H}}}{c^{1.5}} \tag{6}$$

where F is the applied load in Newtons, d is the diagonal of the indent in meters, and 1.854 is the geometric factor used for a square pyramidal indenter tip. In Equation 6, E is the elastic modulus, H is the hardness, and c is the average crack length. Ten indents were made on polished cross sections and crack lengths were excluded if they branched, while entire indents were excluded if chipping occurred, as such indents invalidate the measurement technique. The crack length was averaged for each indent and the standard deviation provided is from a minimum of 7 total indents. The strain energy release rate (Γ) was also calculated to enable comparison to literature values, where:

$$\Gamma = \frac{K_{IFR}^2}{E} \tag{7}$$

It should be noted that there has been debate regarding the utility of the indentation method for measuring fracture toughness. Hence, the values here are reported as indentation fracture resistance (K_{IFR}). While several authors have discussed the numerous potential flaws associated with this technique(17,18), the indentation technique is still useful. It offers the ability to investigate small specimens of samples, provided the guidance from the original description of the technique is followed and understood (19). In the case of this paper, the materials and morphologies being compared are similar and thus the error of comparing materials from different classes is mitigated. Additionally, the similarity of the oxides is expected to produce similar failure, thus further reducing the potential error of the technique. Therefore, even if the magnitude of the resultant fracture resistance may differ from other techniques, the measured difference in values between the samples, or rankings, is still quite relevant.

Particle erosion testing was performed on the pellets using an in-house erosion rig and 50 μm α-Al_2O_3 media. The erosion tests were performed at a particle impact angle of 90°, particle velocity of 100 m/sec and substrate to nozzle distance of 23 cm. The erosive media was fed at a feed rate of 2 g/min in 5 g increments. A total of 50 grams of media was used, resulting in ten mass loss measurements per sample. The process has been described elsewhere in more detail (20).

X-ray diffraction (XRD) θ-2θ scans were employed (PANalytical XPert Pro MPD) and the ICDD Crystallographic Database were used to characterize crystal structure via whole pattern fitting (Jade 10). Scanning electron microscopy and field emission scanning electron microscopy (FEI Quanta 200 ESEM, FEI Nova NanoSEM 630 FESEM) were used to identify and characterize sample morphology and grain size, while energy dispersive spectroscopy (EDS) was performed to determine chemical composition. Characterization of microstructural features such as grain size is important in understanding the behavior of both single phase and multiphase materials, as mechanical properties such as hardness, dislocation motion, and stress-strain relationships depend heavily on grain structure in polycrystalline materials. Methods to determine average grain size for single phase materials are well understood and generally effective; however, few standardized methods exist to characterize the grain structure of multiphase materials. Therefore, the linear intercept method (ASTM E112-13) was used to approximate the grain size of the monolithic GZO and GAP pellets and a separate method was

developed for the composite pellets. This involved image segmentation via ImageJ software combined with EDS compositional analysis. Grain images were first taken in secondary electron (SE) micrographs, while EDS compositional maps of the regions were used to differentiate GZO grains from GAP grains in the composites. The grain boundaries in the micrographs were manually traced to produce sufficient contrast between the grain boundaries and the grains. A threshold was then applied in ImageJ to produce a black and white image of the contrasted grains and grain boundaries. The individual grain areas were then measured in ImageJ and counted. Figure 2 provides images after each step of this process. Because the GZO and GAP grains in both the monolithic and composite pellets were fairly equiaxed, the grain areas were treated as areas of perfect circles, with the sizes being calculated as the diameters of the circles. Through the use of image segmentation and analysis, it was also possible to determine the distribution of the grain sizes from the micrographs, as a distribution of grains in a sample can give important information on sintering and coarsening processes.

3. Results and Discussion

3.1. Sintered Morphology and Density

Cross sectional back scattered SEM of the sintered composite pellets are provided in Figure 3. Two distinct phases were observed, a bright matrix phase (GZO) and a darker interdispersed phase (GAP). In the 90:10 pellet, the GAP phase is well dispersed, and the individual grains exhibit minimal contact with other GAP grains. As the fraction of GAP phase increases, the number of GAP grains in contact increases. This enables some coarsening in the higher GAP fraction composites and an overall increase in the particle size of the GAP phase. The densities of the as-sintered pellets are provided in Table 1 and are all between 97-100% of the calculated theoretical densities, meaning that any changes in mechanical properties observed in the study will reflect changes in composite variation composition and not porosity. Theoretical densities range from 6.94 g/cc for pure GZO to 7.44 g/cc for pure GAP.

Grain size was measured using secondary electron SEM images with example images provided in Figure 4. For the composite pellets, EDS was utilized to confirm the presence of aluminum and the location of the GAP grains, as shown in Figure 4f-h, with the resulting grain size analysis provided in Figure 5 and average grain sizes in Table 1. The GZO grain size (Figure 5a) is initially large and broadly distributed in the monolithic pellet (solid line) with

grain size decreasing and distribution narrowing as GAP is added. Conversely, the GAP grain size (Figure 5b) is initially small though relatively broadly distributed. The wide distribution of grain size in both the monolithic GZO and GAP pellets gives some limited insight into the growth kinetics of the materials, with the larger grains growing at the expense of smaller grains, as opposed to the composite pellets, which overall have much narrower distributions possibly due to limited growth. The lack of coarsening in the composites is attributed to the lack of reactivity between GAP and GZO and thus the limitation of diffusion. The grain size distribution narrows in the composites, with initially small grains for the GAP phase in the 90:10 which become larger as the GAP volume fraction increases, agreeing well with the qualitative observations from the BSE micrographs. However, the overall magnitude of the GAP grain size increase in the composite samples was relatively small, from approximately 1.08 ± 0.37 to 1.43 ± 0.52 µm. The smaller grain size, and thus higher microstructural stability of the composites is a further illustration of the thermochemical stability between the two phases during sintering. This behavior is highly desirable for potential TBC applications, as sintering and grain growth often contribute to TBC failure due to the resultant increases in the coating elastic modulus. These higher moduli yield increased stresses in coatings during thermal cycling and therefore promote failure.

3.2. Phase Stability and Thermomechanical Stability

X-ray diffraction patterns of the sintered monolithic and composite pellets are shown in Figure 6. The pure GAP pellet exhibits an orthorhombic perovskite structure, while the pure GZO pellets exhibit the cubic fluorite structure with very weak pyrochlore ordering noted by the presence of the superstructure peaks denoted in the figure. The weak pyrochlore ordering in the as-sintered state is a result of the 1600°C sintering temperature being above the ~1550°C pyrochlore stability limit. Therefore, atomic ordering only occurs during the short cooling period in the temperature window of approximately 1550°C to 1200°C (i.e., until the temperature is too low for ordering to occur). The XRD patterns in Figure 6 for the composite pellets show a mixture of the perovskite and fluorite/pyrochlore phases, with weight fractions calculated from whole pattern refinement agreeing well with the expected weight ratios listed in Table 1. Additionally, no tertiary GZO-GAP reaction phase was observed in any of the composite pellets, confirming high temperature phase stability between GZO and GAP at 1600°C for 24 hours.

To further demonstrate the phase stability, long term heat treatments were performed at 1425°C for 500 hours with the resulting XRD patterns provided in Figure 7. The monolithic GAP and GZO pellets exhibited the expected orthorhombic and pyrochlore phases, respectively. No reaction was observed in any of the composite pellets over the duration of the heat treatment, in line with the phase equilibria predicted by several authors and provided in Figure 1 (1,14,15).

It should be noted that although several three phase regions are present in the GAP equilibria at 1250°C (blue in Figure 1) (1), practically speaking they have minimal impact on performance as they consist of GAP plus an ordered pyrochlore and disordered fluorite phase. The fluorite and pyrochlore phases from these potential three phase regions are close enough in chemistry to exhibit similar lattice constants and thermomechanical behavior. Thus, they would behave nearly identically and would likely cause minimal stress or disruptive behavior to the material. Furthermore, some studies indicate there is indeed no two phase region between the pyrochlore and fluorite (and thus no three phase region), and that there is a second order transition between fluorite and pyrochlore where ordering continuously occurs (14). Overall, this indicates there is flexibility in the zirconate composition while still maintaining compatibility with GAP. This is important as it enables some flexibility in the processing of the materials. Additionally, previous research has shown that reducing the rare earth content in GZO can slightly increase the fracture toughness and erosion durability (4) with minimal impact on the thermal conductivity (21). Thus, the compositional flexibility enables fine tuning of the composites for higher durability (lower RE content) or higher CMAS resistance (higher RE content).

Importantly, above 1550°C when GZO transitions from the pyrochlore to the fluorite phase, stability is maintained with the GAP phase (1,15). The high temperature fluorite phase exhibits compatibility with GAP across a broad region from about 22 mol% to ~52 mol% Gd_2O_3. The high temperature stability therefore ensures composites of these two materials are capable of even the most demanding TBC environments in terms of thermochemical compatibility, as the stability limit is the ~2045°C melting temperature of GAP.

3.3. Mechanical Properties

Elastic modulus, hardness, and fracture toughness are three critical components affecting the durability of TBCs, both in terms of thermal cyclic life and erosive wear. The elastic

modulus and hardness are provided in Figure 8. The modulus shows a fairly linear reduction from 249 GPa for GZO to 203 GPa for GAP, in line with literature values (22,23). Combined with CTE, the elastic modulus will affect the strain energy stored during thermal cycling and after CMAS infiltration. The stored elastic strain energy (*U*) is given as:

$$U = \frac{1}{2}\frac{V}{E}\sigma^2 \quad (8)$$

where V is the volume, E is the elastic modulus, and σ is the stress. If the strain energy in a coating (or coating layer) is larger than the critical energy release rate, delamination can occur. The amount of stress in the coating layers during thermal cycling is predominantly related to the thermal expansion mismatch stresses, (though gradient stresses also play a role for large gradients). The CTE of GAP is anisotropic and averages around 10.6 ppm/°C, in line with YSZ and GZO. If CTE mismatch occurs, a lower elastic modulus will reduce the mismatch stresses and the total stored strain energy. Therefore, the slightly lower modulus value of GAP will reduce any effects of the CTE mismatch and anisotropy.

In addition to thermal cyclic durability, the erosion durability is also dictated by the mechanical properties. The literature has described the volume loss (*V*) during erosion with the following relation (24):

$$V \propto w_p^{21/20} R_p^{11/3} \rho_p^{21/10} K_{C,c}^{-4/3} H_c^{-1/4} \quad (9)$$

Where w_p, R_p, and ρ_p velocity, radius, and density of the incoming particle, and $K_{C,c}$ and H_c are the fracture toughness and hardness of the coating material. Hardness represents the resistance to plastic deformation and high hardness values typically provide high wear resistance. In terms of erosion, the hardness is related to the depth at which cracking occurs. In brittle failure under spherical contact, higher hardness yields cracking at smaller depths, as the elastic-plastic interface is closer to the surface (24). Although the GAP modulus was lower than GZO, hardness was not sacrificed and was nearly constant at approximately 13 GPa regardless of composite composition. These hardness values are similar to that of YSZ at 14 GPa (25). Thus, there is no expected performance debit based on the hardness of this material which is comparable to most zirconates.

The fracture toughness heavily impacts the erosion resistance as indicated by the $K^{-4/3}$ exponent in Equation 9. The indentation fracture resistance of the sintered pellets is provided in Figure 9 and will herein be referred to as fracture toughness for simplicity. Standard deviations were generally smaller than the data points. The fracture toughness of the GZO sample was

approximately 0.83 MPa√m, agreeing well with literature values (4,7,9). Pure GAP exhibited a fracture toughness of 1.91 MPa√m, over double that of GZO. Equation 9 suggests that these differences in fracture toughness would result in a 67% lower volume loss rate for GAP. As expected, the toughness of the composite samples was intermediate between that of the monolithic samples. The 90:10 sample sits slightly above the trendline while the 70:30 sample falls in line with the predicted trend and the 50:50 sample falls below the trend. This relationship was also observed for the elastic moduli in Figure 8. Griffith's failure criterion indicates that for a given crack length (a), the failure is related to a critical stress σ_c:

$$\sigma_c \approx \left(\frac{2E\gamma}{\pi a}\right)^{1/2} \quad (10)$$

where E is the elastic modulus and γ is the surface energy. The critical stress is proportional to the critical stress intensity factor. Thus, a slightly higher elastic modulus will yield a slightly larger fracture toughness according to Griffith. This assumes the surface energy and crack length are equivalent, both of which are reasonable assumptions for these composites processed under identical conditions.

3.4. Erosion Durability

The erosion data is plotted in Figure 10 as a function of GAP wt.%. Only one sample was tested for each composition, thus error bars can only be based on the standard deviation in the mass changes and are smaller than the data points. Previous work indicates deviations of 5% or less for coatings from a single batch, though this is expected to be lower for dense pellets with fewer microstructural effects. Therefore, care should be taken when comparing small changes between individual values. The pure GZO sample exhibits an erosion rate of 0.622 g/kg while the GAP sample exhibits a much lower erosion rate at 0.245 g/kg. This represents a 61% reduction in the erosion rate with respect to the pure GZO pellet and is tied to the increase in the fracture toughness of GAP. Indeed, the 61% reduction is close to the 67% reduction predicted by Equation 9. As GAP is added to the GZO to produce composite pellets, the erosion rate decreases and approaches a minimum by the 50:50 composition and this minimum is maintained to the GAP sample. The lack of a linear trend in the erosion is somewhat surprising, as erosion is heavily dependent upon the fracture toughness. For these composites, the fracture toughness values were fairly linear. In particular, the fracture toughness of the 50:50 sample was significantly lower than pure GAP, whereas the erosion rates were nearly equal. This suggests

additional toughening behavior is occurring in the composites beyond simply the volumetric addition of a higher fracture toughness material.

Composite behavior is traditionally bound by the Voigt-Reuss conditions, where Voigt represents the upper or linear boundary and Reuss represents the lower or series boundary. In TBCs, the microstructure is highly anisotropic and can produce non-linear effects which yield behavior outside Voigt-Reuss boundaries. However, the pellets should exhibit minimal morphological anisotropy given their dense nature and homogeneous dispersion of roughly spherical particles. Therefore, the composite behavior should be constrained by the Voigt-Reuss boundaries and yet the experimental data lies outside of these boundaries. This further confirms additional effects are occurring outside of a traditional Voigt-Reuss power law average.

One potential contribution to the composite behavior is that the GAP phase provides enhanced toughening in the mixtures via ductile or plastic behavior. Plastic deformation can provide energy absorption at the crack tip and significantly enhance toughness, hence the generally higher values of fracture toughness in metals versus ceramics. Ceramic oxides typically do not exhibit significant ductility or plastic deformation due to their primarily ionic bonding character and the resulting lack of slip. However, plastic deformation has been observed in GAP composites tested at elevated temperatures (1600°C) and was attributed to dislocation motion (26). Unfortunately, this mechanism is only available at elevated temperatures where sufficient energy is available to overcome the energy barrier to form and move dislocations. Another mechanism which provides ductility in ceramics is termed micrograin superplasticity (27) and has been demonstrated for both covalent (28) and ionic ceramics, including YSZ (29–31). This mechanism relies on grain boundary sliding of fine grain structures and is related to the grain boundary diffusivity and surface energy. The grain boundary diffusivity must be sufficiently high to enable movement of grain boundaries which results in a reduction in local stresses. In addition, the boundary-to-surface energy ratio must be low to prevent formation of cavities. Again, this mechanism requires high temperatures to promote diffusion. Since testing in the current study was performed at room temperature, the diffusivities are insufficient to enable grain boundary movement or significant dislocation motion. Furthermore, even at elevated temperature, the timescales for grain boundary motion

may not be compatible with the erosive impact and stress propagation [i]. As a qualitative evaluation of ductile behavior, erosion tests were performed at 30° impingement angles where elastic materials tend to perform best, and ductile materials tend to perform worst. The results were hampered by very low erosion rates for the ceramic materials, however, no significant change in the relative rates was observed. Thus, it appears qualitatively that minimal plasticity is likely to occur at room temperature. Furthermore, if plastic deformation were observed, it would be expected to benefit the pure GAP pellet to a higher degree than the composites. Therefore, even if it were observed, room temperature plasticity would not completely explain why the 50:50 composite pellet exhibited better than expected erosion.

Another potential mechanism which could impact the non-linear erosion results is the effect of grain size. The end member grain sizes are slightly larger and exhibit a broader dispersion compared to the composites. However, it is unlikely that the approximately 2 μm difference in average grain size between the composites and end members would have a substantial effect. Indeed, hardness is sensitive to grain size given the Hall-Petch relationship, and negligible changes were observed between the hardness of the composites and the end members. A related effect could be the crack propagation and crack path tortuosity. The crack path may become more tortuous in the composites and therefore act as an energy sink. Figure 11 provides SEM images of fracture surfaces for each of the pellets. The GZO pellet exhibits transgranular cracking while the GAP pellet exhibits a larger degree of intergranular failure. The 90:10 composite behaves similarly to the GZO but as further GAP is added, the failure mode changes and the surface becomes significantly rougher, i.e. the crack path becomes more tortuous. This can cause crack bridging, skipping and deflection, which was observed in some of the indentation cracks for the 50:50 composite as shown in Figure 11f. Part of this effect could be related to the smaller grain size in the composite samples where GAP promotes intergranular failure and causes crack deflection, resulting in a crack propagation which rapidly and repeatedly changes directions. However, if the crack path tortuosity were to significantly enhance toughening, it should be observed in the indentation results and yet was not.

To establish a mechanism which impacts erosion and not indentation fracture toughness, one must compare loading and failure during the two processes. One key difference is that the

[i] It should be noted, however, that any plasticity that does occur at elevated temperature would be likely be beneficial to the erosion durability as this would significantly enhance the toughness of TBCs during elevated temperature operation.

erosion process is dynamic and experiences very high transient stresses. A second is that erosion is not a measure of cracking, but of material removal. Therefore, to cause a change in erosion that is not observed in indentation, the material or structural changes must impact transient stress development and/or material removal. As previously mentioned, crack bridging and crack skipping were observed. It is hypothesized that these may have a greater impact on the erosion process by preventing material removal and requiring successive impacts for removal of previously fractured regions. Thus, the 50:50 samples which has the smallest grain size and greatest degree of crack path tortuosity may yield the largest amount of bridging and skipping. Further study is required to confirm the mechanism behind the improved erosion relative to fracture toughness.

3.5. Implications for TBC Applications

The results provide a number of implications regarding GZO-GAP composites for TBC applications. First, it has been confirmed that the mechanical properties are significantly enhanced with respect to GZO, and thus the GAP phase can act as a toughening agent. Importantly, this composite is one of the first TBC material systems which is capable of elevated temperature operation beyond 1400°C for prolonged duration while exhibiting good erosion durability. Additionally, if the elevated temperature plasticity reported in the literature for GAP is experienced during high temperature erosion, this could further enhance the durability of GZO-GAP composites.

Outside of the mechanical properties investigated in this report, thermal conductivity and thermal cyclic durability represent two additional pillars of TBC performance. The thermal conductivity of GAP is not well established, however, available literature for $LaAlO_3$ indicated a value of approximately 1.9 W/m·K at elevated temperature (32). The sole paper exploring GAP indicates a value of approximately 3.2 W/m·K at elevated temperatures (33). However, in previous studies it was found that the thermal conductivity of the toughening phase had a minor effect on the thermal conductivity of GZO-based composite coatings (10,11). This response has been observed for bulk ceramic composites of other materials such as Al_2O_3 and mullite in YSZ (34), indicating series-like behavior. This series behavior is expected for lamellar air plasma spray (APS) splat morphologies and thermal conduction normal to the splat alignment, which further reinforces the observation that the thermal conductivity of the secondary toughening

phase does not necessarily need to be as low as the primary matrix phase, especially at small volume fractions. Due to the non-linear effects of GAP additions on erosion behavior, it is anticipated that low volume fractions can be utilized and thus that thermal conductivity will not be sacrificed. Furthermore, the thermal conductivity can be heavily modified by manipulating the morphology. This is one factor which will be assessed in coatings in future work. Additionally, the effect of GAP additions on thermal cyclic durability will be evaluated to determine if the anisotropic CTE of GAP has a negative effect. Air plasma spray coatings are currently being fabricated to enable evaluations of these properties.

An additional benefit of incorporating GAP or other aluminates as a toughening phase is the low oxygen diffusivity in these materials. For example, the oxygen diffusivity of $Y_3Al_5O_{12}$ (YAG) is on the order of 10^{-20}-10^{-25} m^2/s compared to YSZ at 10^{-10} – 10^{-11} m^2/s (35). A low oxygen diffusivity can help reduce the growth rate of the TGO layer. This is an important factor, because even if CMAS, erosion, and thermal cyclic durability are all satisfied, failure will eventually occur due to TGO growth. Thus, a low oxygen diffusivity can further enhance the overall durability of the TBC system.

One of the last critical factors for next generation TBCs is the resistance to degradation caused by infiltration of molten CMAS deposits. Work is currently being performed to evaluate the CMAS resistance of the GZO-GAP composites with initial results suggesting GAP is equivalent to, or potentially more CMAS resistant than, GZO. This is due to a propensity to efficiently form large amounts of reaction phases at high rates.

4. Conclusions and Future Work

This work provides a new strategy for the development of next generation TBC materials by combining a low conductivity, high thermal stability zirconate material with a thermochemically compatible and phase stable aluminate toughening material. It was demonstrated that:

- GAP and GZO are phase stable in contact through 1600°C.
- The fluorite/pyrochlore phase transformation does not impact the stability between GZO and GAP.
- GAP enhances the mechanical properties of the composites by reducing modulus, maintaining hardness, and more than doubling fracture toughness.

- Integrating GAP successfully reduces the erosion rate by over 61% with respect to GZO.
- Non-linear effects occur in GZO-GAP composites where small additions of GAP can produce significant enhancement in erosion durability.

Overall, this study indicates that GZO-GAP composites can provide enhanced durability and thermal stability with small additions of GAP providing significant improvement in the erosion resistance. Several potential mechanisms were identified which may contribute to these non-linear effects. Future work will attempt to target these mechanisms to determine the cause of the non-linear behavior and potentially enable tailoring and enhancement of this behavior. It is envisioned that varying the average grain sizes through heat treatments may yield different degrees of crack bridging and skipping and enable investigation of these effects. Concurrent work focusing on the CMAS resistance of the GAP material and GZO-GAP composites is in progress and shows significant promise. Additionally, GZO-GAP composite coatings are being fabricated for future work, which will evaluate the thermal cyclic durability, thermal conductivity, and erosion durability. This will enable assessments of the effect of GAP in coating microstructures and the transition from dense fine-grained composites to porous splat morphologies, as well as evaluation of properties that are not easily or feasibly tested in bulk pellets, such as thermal cyclic durability.

5. Acknowledgements

The authors would like to acknowledge Brenna Gorin for her assistance in early fabrication and testing. This research was sponsored in part by a Department of Energy (DoE) STTR award number DE-SC0004356 under the supervision of Dr. Patchrin Burke. Any opinions, findings, conclusions, or recommendations expressed in this material are those of the authors and do not necessarily reflect the views of the US DoE.

6. References

1. Lakiza S, Fabrichnaya O, Wang C, Zinkevich M, Aldinger F. Phase diagram of the ZrO_2–Gd_2O_3–Al_2O_3 system. J Eur Ceram Soc. 2006;26(3):233–46.
2. Maloney MJ. Thermal Barrier Coating Systems and Materials. United States; U.S. Patent No. 6,177,200, 2001.
3. Krämer S, Yang J, Levi CG. Infiltration-inhibiting reaction of gadolinium zirconate thermal barrier coatings with CMAS melts. J Am Ceram Soc. 2008;91(2):576–83.
4. Schmitt MP, Stokes JL, Gorin BL, Rai AK, Zhu D, Eden TJ, et al. Effect of Gd content on mechanical properties and erosion durability of sub-stoichiometric $Gd_2Zr_2O_7$. Surf Coatings Technol. 2017;313:177–83.
5. Schmitt MP, Rai AK, Bhattacharya R, Zhu D, Wolfe DE. Multilayer thermal barrier coating (TBC) architectures utilizing rare earth doped YSZ and rare earth pyrochlores. Surf Coatings Technol. 2014;251:56–63.
6. Rai AK, Schmitt MP, Dorfman MR, Zhu D, Wolfe DE. Comparison of single-phase and two-phase composite thermal barrier coatings with equal total rare-earth content. J Therm Spray Technol. 2018;25(4):556–65.

7. Zhang Y, Guo L, Zhao X, Ye F. Effects of non-stoichiometry on the mechanical properties of Nd2−xZr2+xO7+x/2 (x=0, 0.1, 0.2, 0.3, 0.4, 0.5) ceramics. Mater Lett. 2014;136:157–9.

8. Guo L, Li M, Zhang Y, Ye F. Improved toughness and thermal expansion of non-stoichiometry Gd2−xZr2+xO7+x/2 ceramics for thermal Barrier Coating Application. J Mater Sci Technol. 2016;32(1):28–33.

9. Wang C, Guo L, Zhang Y, Zhao X, Ye F. Enhanced thermal expansion and fracture toughness of Sc2O3-doped Gd2Zr2O7 ceramics. Ceram Int. 2015;41(9):10730–5.

10. Schmitt MP, Rai AK, Zhu D, Dorfman MR, Wolfe DE. Thermal conductivity and erosion durability of composite two-phase air plasma sprayed thermal barrier coatings. Surf Coatings Technol. 2015;279:44–52.

11. Schmitt MP, Schreiber JM, Rai AK, Eden TJ, Wolfe DE. Development and optimization of tailored composite TBC design architectures for improved erosion durability. J Therm Spray Technol. 2017;26(6):1062–75.

12. Rai AK, Schmitt MP, Bhattacharya RS, Zhu D, Wolfe DE. Thermal conductivity and stability of multilayered thermal barrier coatings under high temperature annealing conditions. J Eur Ceram Soc. 2015 May;35(5):1605–12.

13. Panneer Selvam M, Rao KJ. Microwave synthesis and consolidation of gadolinium aluminum perovskite, a ceramic extraordinaire. Adv Mater. 2000;12(21):1621–4.

14. Leckie RM, Krämer S, Rühle M, Levi CG. Thermochemical compatibility between alumina and ZrO2–GdO3/2 thermal barrier coatings. Acta Mater. 2005 Jun;53(11):3281–92.

15. Fabrichnaya O, Seifert HJ. Up-Date of a Thermodynamic database of the ZrO_2-Gd_2O_3-Y_2O_3-Al_2O_3 system for TBC applications. J Phase Equilibria Diffus. 2011;32(1):2–16.

16. Panneerselvam M, Aggarwal N, Subanna GN, Rao KJ. GdAlO3–ZrO2: A ductile ceramic composite. Adv Eng Mater. 2003;5(4):243–6.

17. Antsis G. R, Chantikul P, Lawn BR, Marshall DB. A critical evaluation of indentation

techniques for measuring fracture toughness: I, direct crack measurements. J Am Ceram Soc. 1981;64(9):533–8.

18. Quinn GD, Bradt RC. On the vickers indentation fracture toughness test. J Am Ceram Soc. 2007;90(3):673–80.

19. Marshall DB, Cook RF, Padture NP, Oyen ML, Pajares A, Bradby JE, et al. The compelling case for indentation as a functional exploratory and characterization tool. J Am Ceram Soc. 2015;98(9):2671–80.

20. Wolfe DE, Schmitt MP, Zhu D, Rai AK, Bhattacharya R. Multilayered thermal barrier coating architectures for high temperature applications. In: Zhu D, Lin H-T, Zhou Y, Hwang T, editors. 37th International Conference on Advanced Ceramics and Composites: Advanced Ceramic Coatings and Materials for Extreme Environments. Hoboken, NJ: John Wiley and Sons, Inc.; 2013. p. 3–18.

21. Wu J, Padture NP, Klemens PG, Gell M, Miranzo P, Osendi MI. Thermal conductivity of ceramics in the ZrO2 -GdO1.5 system. J Mater Res. 2002;17(12):3193–200.

22. Bass JD. Elasticity of single-crystal $SmAlO_3$, $GdAlO_3$ and $ScAlO_3$ perovskites. Phys Earth Planet Inter. 1984;36(2):145–56.

23. Shimamura K, Arima T, Idemitsu K, Inagaki Y. Thermophysical properties of rare-earth-stabilized zirconia and zirconate pyrochlores as surrogates for actinide-doped zirconia. Int J Thermophys. 2007;28(3):1074–84.

24. Aquaro D, Fontani E. Erosion of ductile and brittle materials. Meccanica. 2001;36(6):651–61.

25. Schaedler TA, Leckie RM, Krämer S, Evans AG, Levi CG. Toughening of nontransformable t'-YSZ by addition of titania. J Am Ceram Soc. 2007;90(12):3896–901.

26. Waku Y, Nakagawa N, Wakamoto T, Ohtsubo H, Shimizu K, Kohtoku Y. A ductile ceramic eutectic composite with high strength at 1,873K. Lett to Nat. 1997;389(6646):49–52.

27. Evans AG, Rice JR, Hirth JP. Suppression of cavity formation in ceramics: prospects for

superplasticity. J Am Ceram Soc. 1980;63(7–8):368–75.

28. Wakai F, Kodama Y, Sakaguchi S, Murayama N, Izaki K, Niihara K. A superplastic covalent crystal composite. Lett to Nat. 1990;344(6265):421–3.

29. Wakai F, Sakaguchi S, Matsuno Y. Superplasticity of yttria- stabilized tetragonal ZrO_2 polycrystals. Adv Ceram Mater. 1986;1(3):259–63.

30. Wakai F, Kato H. Superplasticity of TZP/Al_2O_3 composite. Adv Ceram Mater [Internet]. 1988;3(1):71–6. Available from: http://www.msl.titech.ac.jp/~dfc/pdf/SCI 161.pdf

31. Betz U, Padmanabhan KA, Hahn H. Superplastic flow in nanocrystalline and sub-microcrystalline yttria-stabilized tetragonal zirconia. J Mater Sci. 2001;36(24):5811–21.

32. Suresh G, Seenivasan G, Krishnaiah M., Murti PS. Investigation of the thermal conductivity of selected compounds of lanthanum, samarium and europium. J Alloys Compd. 1998;269(1–2):L9–12.

33. Suresh G, Seenivasan G, Krishnaiah MV, Srirama Murti P. Investigation of the thermal conductivity of selected compounds of gadolinium and lanthanum. J Nucl Mater. 1997 Oct;249(2–3):259–61.

34. Angle JP, Wang Z, Dames C, Mecartney ML. Comparison of two-phase thermal conductivity models with experiments on dilute ceramic composites. J Am Ceram Soc. 2013;96(9):2935–42.

35. Su YJ, Trice RW, Faber KT, Wang H, Porter WD. Thermal conductivity, phase stability, and oxidation resistance of $Y_3Al_5O_{12}$ (YAG)/ Y_2O_3 – ZrO_2 (YSZ) thermal-barrier coatings. Oxid Met. 2004;61(314):253–71.

Table 1. Pellet weight and volume fractions, sintered densities, and calculated weight fractions via whole pattern fitting.

Sample	GAP wt.%	GAP vol.%	Theoretical Density (g/cc)	Measured Density (% TD)	WPF Composition (GZO:GAP)	GZO Grain Size (µm)	GAP Grain Size (µm)
GZO	0	0	6.94	99.5	100:0	3.09 ± 1.65	--
90:10	10	9	6.99	99.5	89:11	2.62 ± 1.23	1.08 ± 0.37
70:30	30	29	7.08	99.0	68:32	1.36 ± 0.68	1.32 ± 0.44
50:50	50	48	7.18	99.3	54:46	1.21 ± 0.59	1.43 ± 0.52
GAP	100	100	7.44	98.7	0:100	--	2.65 ± 2.09

Figure 1. Ternary Gd_2O_3-ZrO_2-Al_2O_3 phase diagram at 1250°C, with the GZO-GAP phase equilibrium highlighted in green. P = Pyrochlore, F= Fluorite, GAP = $GdAlO_3$, GAM = $Gd_4Al_2O_9$, C = cubic Gd_2O_3, T = Tetragonal ZrO_2. Diagram modified from (1).

Figure 2. Image segmentation process for grain size analysis, with a) original SE micrograph, b) micrograph with traced grain boundaries, c) black and white threshold image and d) final grain count produced by ImageJ.

Figure 3. BSE micrographs of polished cross sections of a) 90:10, b) 70:30, and c) 50:50 GZO-GAP composite pellets. The darker phase in the micrographs was identified as GAP through EDS analysis. Pullout occurred during polishing resulting in some porosity appearing at the surface.

Figure 4. SE micrographs of grain structure of the pellet surfaces: a) GZO, b) GAP, c) 90:10, d) 70:30 and e) 50:50. The color-coded EDS maps to the right of the micrographs indicate the

location of the GAP grains in the microstructure, as evidenced by the presence of aluminum in the EDS scans corresponding to f) 90:10, g) 70:30, h) 50:50.

Figure 5. Graphs of grain size distribution in the GZO-GAP monolithic and composite pellets for the a) GZO and b) GAP phases.

Figure 6. XRD patterns of as-sintered: a) GZO, b) 90:10, c) 70:30, d) 50:50 and e) GAP pellets.

Figure 7. XRD patterns of the: a) GZO, b) 90:10, c) 70:30, d) 50:50 and e) GAP pellets heat treated at 1425°C for 500 hours.

Figure 8. Elastic modulus and hardness for the monolithic and composite GZO-GAP pellets. The elastic modulus trends linearly with GAP additions, while the hardness of GZO-GAP composites remains relatively constant.

Figure 9. a) Backscattered SEM micrograph of the 50:50 GZO-GAP composite sample, showing a typical indent used to measure K_{IFR}. b) Plot of K_{IFR} as a function of GAP wt.%, demonstrating an increase in the fracture resistance with additions of GAP to GZO.

Figure 10. Mass loss erosion plot of GZO-GAP pellets as a function of GAP vol.%. The pure GZO exhibits an erosion rate nearly 3X higher than that of the 50:50 GZO-GAP composite pellet.

Figure 11. Backscattered SEM fracture surface images of a) GZO, b) GAP, c) 90:10, d) 70:30, and e) 50:50. The GZO exhibits transgranular failure while the GAP exhibits a significant amount of intergranular failure. A polished surface image of the indent crack for f) the 50:50 GZO-GAP composite sample shows crack propagation with transgranular cracking in the GZO phase (light), and intergranular cracking around the GAP phase (dark). The crack deflection in the composites could be partly responsible for the increased erosion durability.

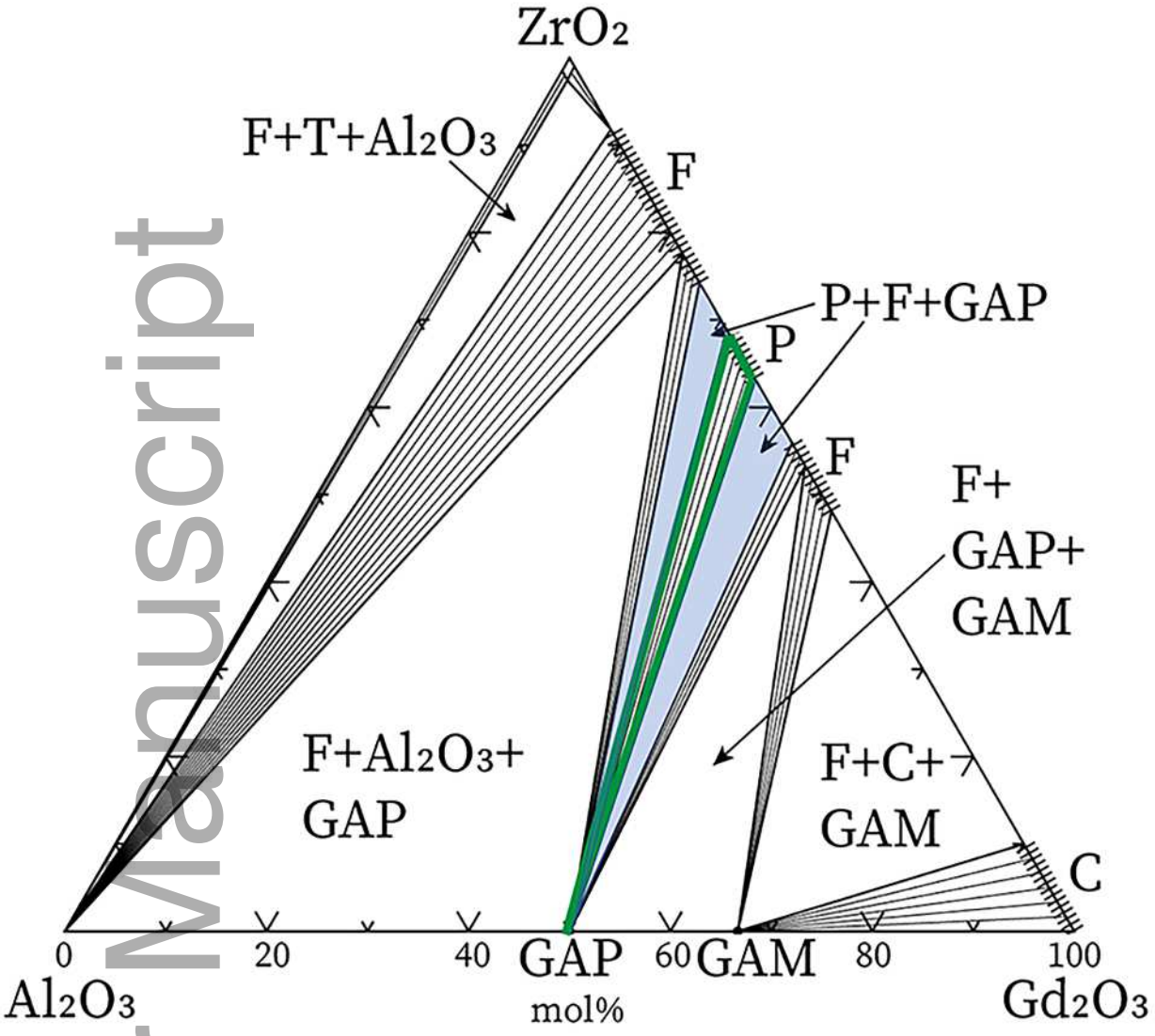

jace_16317_f1.tif

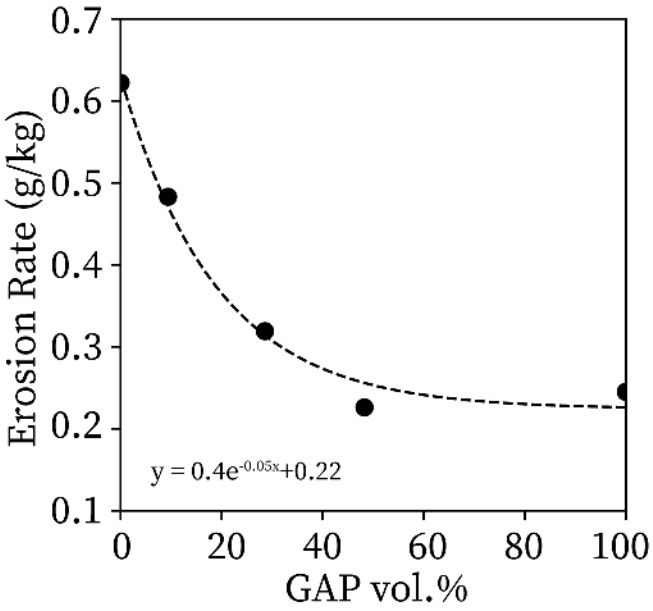

jace_16317_f10.tif

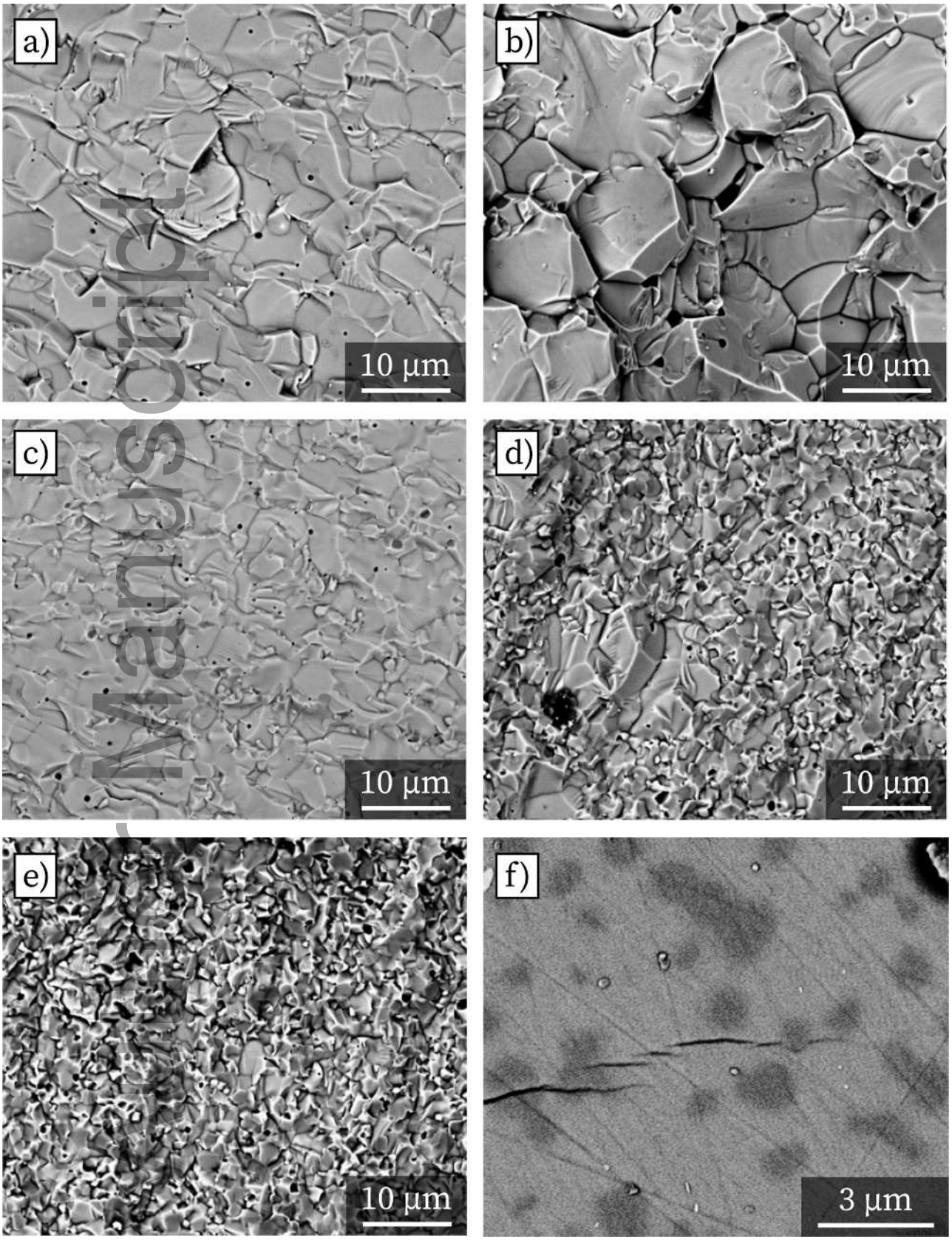

jace_16317_f11.tif

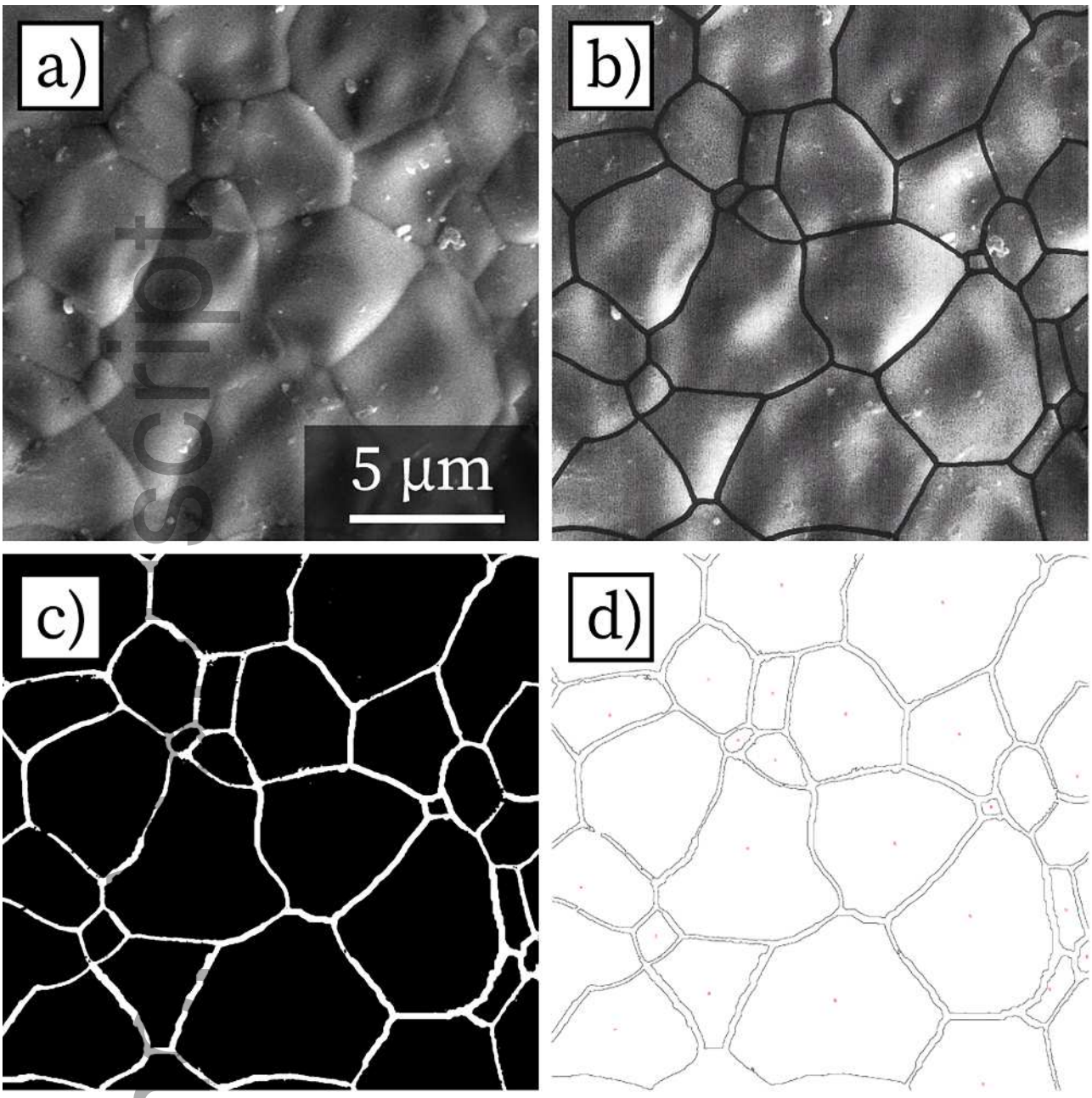

jace_16317_f2.tif

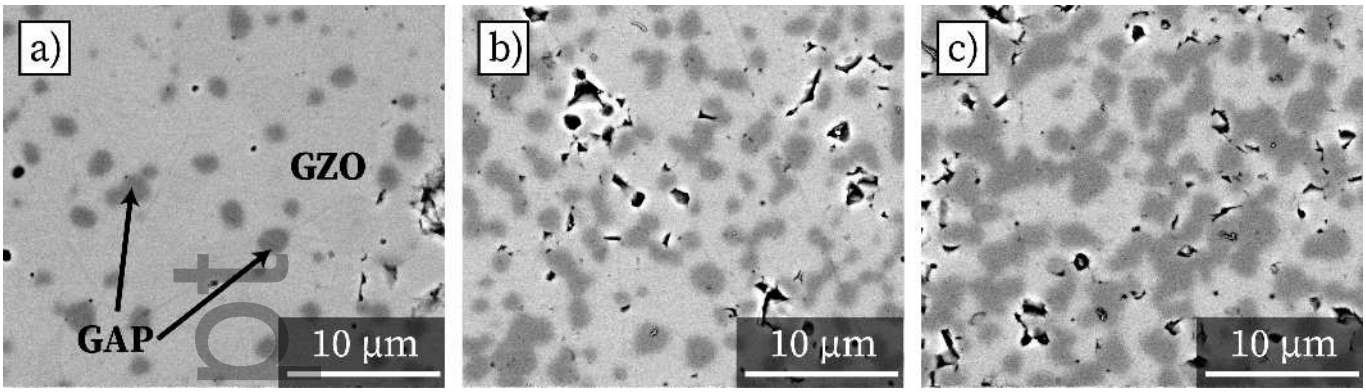

jace_16317_f3.tif

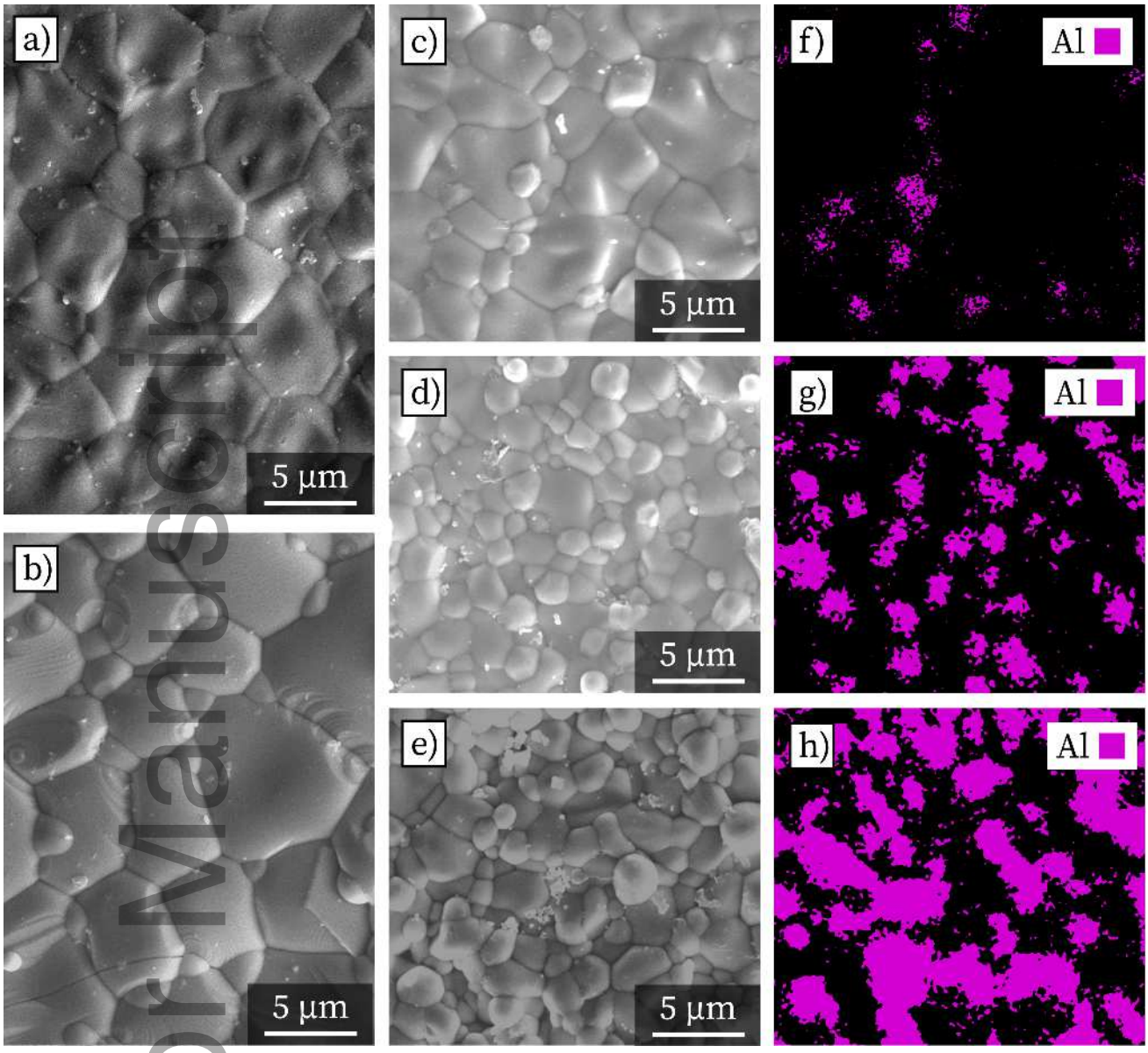

jace_16317_f4.tif

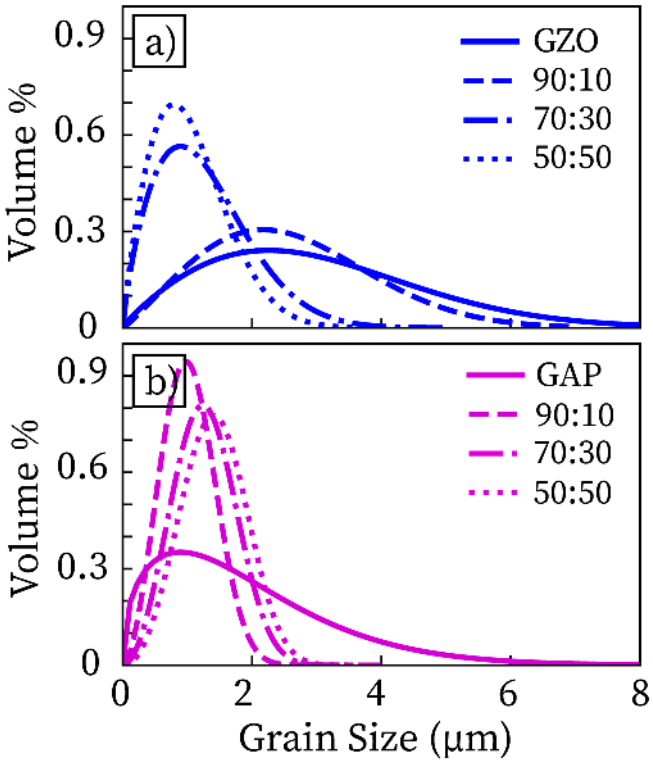

jace_16317_f5.tif

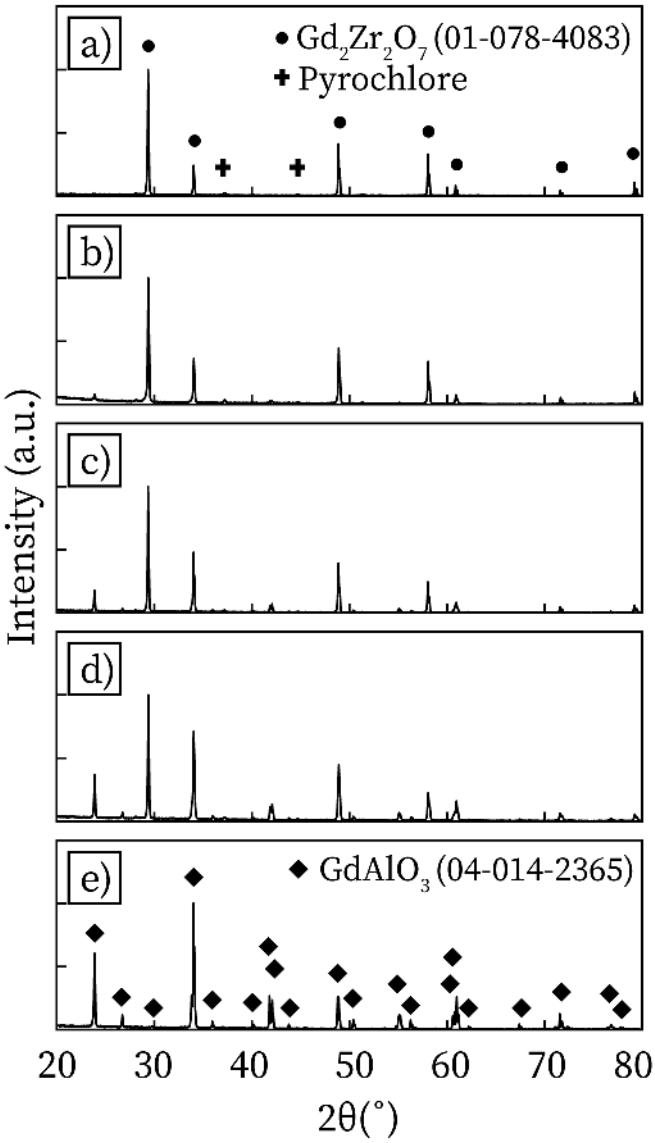

jace_16317_f6.tif

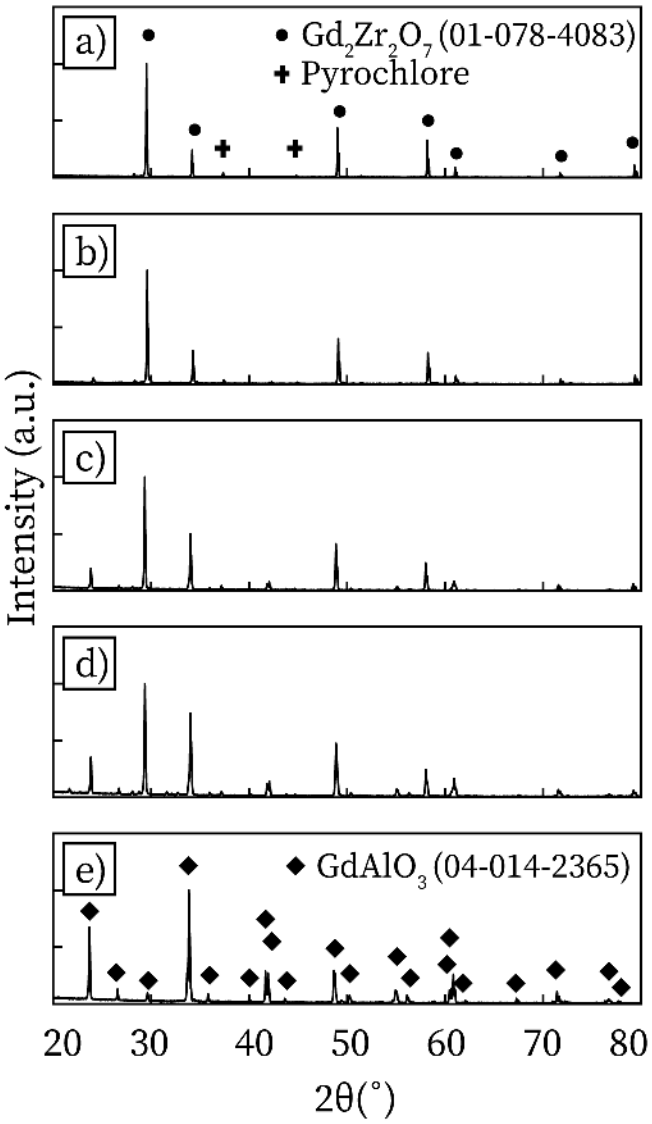

jace_16317_f7.tif

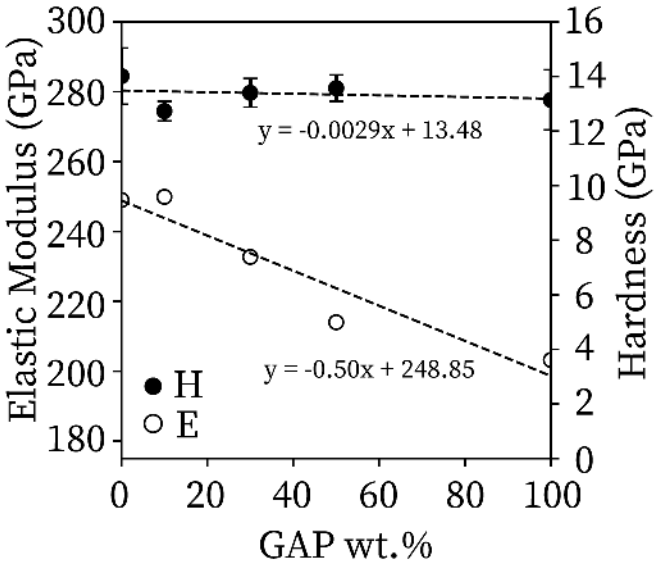

jace_16317_f8.tif

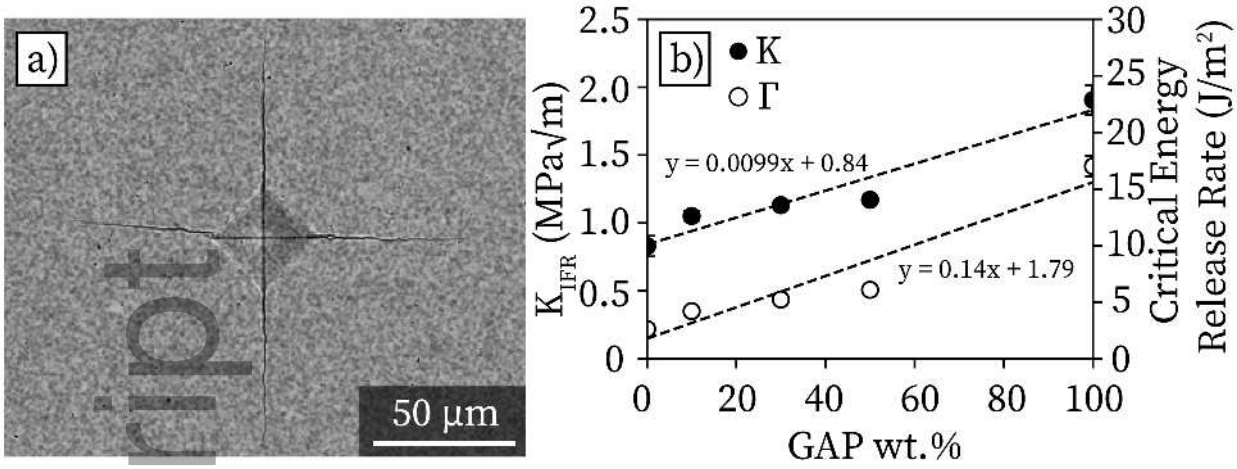

jace_16317_f9.tif